HHS Public Access

Author manuscript

Int J Min Sci Technol. Author manuscript; available in PMC 2021 September 21.

Published in final edited form as:

Int J Min Sci Technol. 2020 September ; 30(5): 635–641. doi:10.1016/j.ijmst.2020.05.012.

Transport model for shale gas well leakage through the surrounding fractured zones of a longwall mine

Kayode M. Ajayi[*], **Steven J. Schatzel**

Centers for Disease Control and Prevention, National Institute for Occupational Safety and Health, Pittsburgh, PA 15236, USA

Abstract

The environmental risks associated with casing deformation in unconventional (shale) gas wells positioned in abutment pillars of longwall mines is a concern to many in the mining and gas well industry. With the recent interest in shale exploration and the proximity to longwall mining in Southwestern Pennsylvania, the risk to mine workers could be catastrophic as fractures in surrounding strata create pathways for transport of leaked gases. Hence, this research by the National Institute for Occupational Safety and Health (NIOSH) presents an analytical model of the gas transport through fractures in a low permeable stratum. The derived equations are used to conduct parametric studies of specific transport conditions to understand the influence of stratum geology, fracture lengths, and the leaked gas properties on subsurface transport. The results indicated that the prediction that the subsurface gas flux decreases with an increase in fracture length is specifically for a non-gassy stratum. The sub-transport trend could be significantly impacted by the stratum gas generation rate within specific fracture lengths, which emphasized the importance of the stratum geology. These findings provide new insights for improved understanding of subsurface gas transport to ensure mine safety.

Keywords

Subsurface gas transport; Longwall mining; Shale gas well; Analytical modeling; Environmental risk; Shale gas casing failure

1. Introduction

The increasing trend of shale gas production has created more awareness of environmental risk, such as explosions and contamination to water aquifers [1–10]. An analysis of compliance reports from gas wells in Pennsylvania shows that a gas well casing and/or

[*]Corresponding author at: 626 Cochrans Mill Road, Pittsburgh, PA 15236, USA. ony2@cdc.gov (K.M. Ajayi).

Declaration of Competing Interest

The authors declare that they have no known competing financial interests or personal relationships that could have appeared to influence the work reported in this paper.

cement failure occurs more often in an unconventional gas well than in a conventional gas well [11,12]. As a result, studies have focused on contamination to groundwater aquifers [10,13–19] and explosions in gas well sites/nearby locations [4,20]. However, there is limited focus on worker's safety in surrounding longwall mines even though some gas wells have been drilled in vicinity of current or future longwall mines in Pennsylvania, West Virginia, Ohio, Virginia, and Tennessee [21]. In addition, mining depth varies in these locations and Western Marcellus depth could vary from 609.6 m to more than 2743.2 m [22]. Therefore, this study focuses on predicting the impact of gas well casing failure on worker's safety in a nearby longwall mine. Longwall or room-and-pillar mining creates a varying degree of deformation [23], such as separation along the bedding planes and shear failure, which induces bending and rock fracturing in the overburden [24]. The overburden strata is classified into the cave zone, the fractured zone, the continuous deformation zone, and the soil zone [23,25] with dimensions related to the seam height. The mining-induced fractured zone can extend up to 145 m [26], and can become a gas flow channel for gassy coal-bearing strata [27–29]. Consequently, the porosity and permeability are altered as longwall mining could induce over a 1000-fold increase in permeability [30] with chances of a 50-mD (millidarcy) increase for a shear failure along the bedding plane [31].

Fig. 1 shows a schematic of a site in Southwestern Pennsylvania with a shale gas well, longwall mine, shale composite, and coal seam; a detailed lithology with the composite layers and thicknesses has been studied previously [29,32]. Findings from related studies show that the gas well casing failure (as represented in Fig. 2) could occur in three horizons: 0–30 m above the mine roof, 0–10 m below the mine floor, and within the overlying coal seam (highlighted in Fig. 1) [33]. If this occurs, the high-pressure gas finds its way through the paths of least resistance and could connect to pre-existing geological faults or fractures [34], which increases the risk of explosions in the mine (arrow direction in Fig. 1). The fire and explosions that occurred in Hutchinson, Kansas (January 17, 2001) are linked to subsurface migration of leaked gas for over 11 km, which resulted in two deaths and loss of properties [34]. Nevertheless, sometimes the surrounding rock formation has low permeability, but some of the gas could make it into the high-permeability fractured zone, which increases the methane concentration in the gob. This could lead to higher methane concentration in the longwall returns and bleeders, which could jeopardize compliance with mandated methane concentrations [35]. Hence, it is important for the mine workers to proactively plan the ventilation design to accommodate these conditions to ensure safety.

To investigate this condition, the produced shale gas is modeled as methane, since it is the predominant constituent [1,36] and the potential gas transport conditions are classified into two types based on flow regime:

1. The first is transport governed by advection, which occurs if the high-pressure gas connects to the fracture network. Transport due to diffusion is negligible compared to advection [37]; the combination of cubic law and Darcy's equation are applied to predict the boundary flow rates and permeability.
2. The second is flow governed by advection and diffusion and is often regarded as low-velocity flow [37]. This is mostly in relatively low-permeability environments or if the gas has lost most of its pressure before connecting

to the fracture network. The gas flux might be low, but it could jeopardize compliance with mandated methane concentrations in returns and bleeders [35,38] or increase the risk of explosion.

As a starting point, this study focuses on developing an analytical model of the second transport scenario considering both advection and diffusion [39,40]. The hypothesis is that the methane flux from a compromised casing could jeopardize compliance with mandated methane concentrations, which impacts safety. Therefore, the focus areas are: (1) predicting changes to the gas flux for transport through fractures in a gassy or non-gassy bearing stratum, and (2) determining if the gas flux could significantly increase the methane concentration in the gob. These findings will provide prior information for effective mine ventilation design in locations with shale gas wells to ensure safety. To investigate this hypothesis, the equations for the gas transport through a single fracture and applications to a discrete fracture network (DFN) are presented in Section 2. The results and discussions are presented in Section 3, and the conclusion and future works are presented in Section 4.

2. Research approach

2.1. Gas concentration along a single fracture

The approach used in this study is to predict gas transport through a single fracture, and then expand this into a DFN model. The equation for contaminant transport through a single fracture is given as [41]

$$\partial c/\partial t = \nabla \cdot (D\nabla c) - \nabla \cdot (Vc) - \lambda c + q \tag{1}$$

where c is the gas concentration in kg/m^3; t the time in s; V the velocity vector in m/s; D the gas diffusion coefficient through the medium in m^2/s; λ the decay rate in 1/s, which could represent the bacterial attenuation of methane in subsurface through oxidation [42]; and q the stratum's gas generation rate in kg/m^{3}s as illustrated in Fig. 3. The three components of the strata gas content are lost gas, desorbed gas, and residual gas [43]. In this case, q represents methane desorption from the strata into the fracture or could be further described as gas flux per unit aperture from the wall of the fractures. However, in some cases, the rock acts as a medium of transport with no emissions from the strata.

Assuming steady, one-dimensional gas transport, and negligible gas attenuation/adsorption, Eq. (1) is simplified as

$$D\left(d^2c/dz^2\right) - u(dc/dz) + q = 0 \tag{2}$$

where u is the advection velocity in m/s. Considering a length of fracture, L in m, and solving Eq. (2) with boundary conditions, $c(0) = c_0$ and $c(L) = c_L$, as illustrated in Fig. 3, the gas concentration is derived as

$$c(z) = c_0 e^{uz/D} + \left(\left(c_L - c_0 e^{uL/D} - qL/u\right)/\left(1 - e^{uL/D}\right)\right)\left(1 - e^{uz/D}\right) + qz/u \tag{3}$$

Eq. (3) is then used with equations of diffusion and advection to predict the gas flux.

2.2. Flux through a single fracture

Assuming gas transport by advection and diffusion (Fick's first law of diffusion), the total flux, J in kg/m^{2}s, is derived as

$$J(L) = u\left(\left(c_{\mathrm{L}} - c_0 e^{\Psi} - qL/u\right)/\left(1 - e^{\Psi}\right)\right) + q(L - D/u) \tag{4}$$

where $\Psi = uL/D$.

2.3. Flux through a discrete fracture network

Transport through a single fracture as presented in Section 2.2 is based on methods developed previously [44–47], however, transport through the fractured zone is through a fracture network. Therefore, this study develops the application of the derived equations to a discrete fracture network. Using Fig. 4 as a case study for this DFN study, nodes 1–7 are external nodes with assumed known concentrations, and nodes 8–13 are internal nodes with unknown concentrations. The internal node concentrations are required and are calculated using mass balance at the internal nodes.

$$\sum_{j=1}^{n} J_{j-i} = 0 \tag{5}$$

For flux from node j to i, Eq. (4) is rewritten as

$$\begin{aligned} J_{j-i} = {} & \left(u_{j-i}/\left(1 - e^{\Psi_{j-i}}\right)\right)c_i - \left(u_{j-i}e^{\Psi_{j-i}}/\left(1 - e^{\Psi_{j-i}}\right)\right)c_j \\ & + q_{j-i}\left(L_{j-i} - L_{j-i}/\left(1 - e^{\Psi_{j-i}}\right) - D/u_{j-i}\right) \end{aligned} \tag{6}$$

By assuming Eqs. (7)–(9), Eq. (6) is simplified and rewritten as Eq. (10).

$$\mu_{j-i} = u_{j-i}/\left(1 - e^{\Psi_{j-i}}\right) \tag{7}$$

$$Y_{j-i} = u_{j-i}e^{\Psi_{j-i}}/\left(1 - e^{\Psi_{j-i}}\right) \tag{8}$$

$$\xi_{j-i} = q_{j-i}\left(L_{j-i} - L_{j-i}/\left(1 - e^{\Psi_{j-i}}\right) - D/u_{j-i}\right) \tag{9}$$

$$J_{j-i} = \mu_{j-i}c_i - Y_{j-i}c_j + \xi_{j-i} \tag{10}$$

For example, at node 10, Eq. (5) is applied to obtain

$$\begin{aligned} & \mu_{1-10}c_{10} - Y_{1-10}c_1 + \xi_{1-10} + \mu_{8-10}c_{10} - Y_{8-10}c_8 + \xi_{8-10} + \mu_{2-10}c_{10} \\ & - Y_{2-10}c_2 + \xi_{2-10} = 0 \end{aligned} \tag{11}$$

By applying a mass balance (Eq. (5)) to all internal nodes in Fig. 4, the final form of the equations is expressed in the form of $AX = B$.

$$\begin{pmatrix} \mu_{10-8}+\mu_{6-8}+\mu_{9-8}+\mu_{11-8} & -Y_{9-8} & -Y_{10-8} & -Y_{11-8} & 0 & 0 \\ -Y_{8-9} & \mu_{8-9}+\mu_{7-9} & 0 & 0 & 0 & 0 \\ -Y_{8-10} & 0 & \mu_{1-10}+\mu_{8-10}+\mu_{2-10} & 0 & 0 & 0 \\ -Y_{8-11} & 0 & 0 & \mu_{5-11}+\mu_{12-11}+\mu_{8-11} & -Y_{12-11} & 0 \\ 0 & 0 & 0 & -Y_{11-12} & \mu_{13-12}+\mu_{11-12} & -Y_{13-12} \\ 0 & 0 & 0 & 0 & -Y_{12-13} & \mu_{3-13}+\mu_{4-13}+\mu_{12-13} \end{pmatrix} \begin{pmatrix} c_8 \\ c_9 \\ c_{10} \\ c_{11} \\ c_{12} \\ c_{13} \end{pmatrix} = \begin{pmatrix} -\xi_{10-8}-\xi_{6-8}-\xi_{9-8}-\xi_{11-8}+Y_{6-8}c_6 \\ -\xi_{8-9}-\xi_{7-9}+Y_{7-9}c_7 \\ -\xi_{1-10}-\xi_{8-10}-\xi_{2-10}+Y_{1-10}c_1+Y_{2-10}c_2 \\ -\xi_{5-11}-\xi_{12-11}-\xi_{8-11}+Y_{5-11}c_5 \\ -\xi_{13-12}-\xi_{11-12} \\ -\xi_{3-13}-\xi_{4-13}-\xi_{12-13}+Y_{3-13}c_3-Y_{4-13}c_4 \end{pmatrix} \quad (12)$$

Thus, the internal node concentrations are calculated from Eq. (12). Eq. (4) is then applied to each of the boundary fractures, and the total boundary flux, J_b, is calculated as

$$J_b = \sum_{j=1}^{n} J_{j-i} A_{j-i} / A_b \quad (13)$$

where n is the number of fractures connecting the boundary; A_{j-i} the fracture area in m^2; and A_b the boundary area in m^2. For example, in Fig. 4, the boundaries are labeled as B1-B4. For flux through B4, $n = 2$, and the fractures are J_{8-6} and J_{9-7}. For this two-dimensional model, the fracture area is the aperture size, and the boundary area is the boundary length at a unit distance normal to the flow plane [48]. The aperture used are assumed to be the hydraulic aperture which produces the same flow rate as a rough-walled fracture under the same pressure gradient [49–51]. Fracture apertures are dependent on vertical/horizontal tension and compression due to stress on the strata [30,52] and could vary across the fracture length [53]. This variation could be implemented using stress-based aperture distribution [54,55] or lognormal distribution proven to replicate aperture values under different stress conditions [52].

2.4. Advection velocity

The advection velocity (u in Eq. (4)) is obtained from the cubic law [56,57].

$$Q = -\rho g b^3 (12\mu)^{-1} \cdot \nabla h \cdot H \quad (14)$$

where Q is the volume flow rate in m^3/s; ∇h the pressure head gradient; b the fracture aperture in m; g the acceleration due to gravity in m/s^2; μ the dynamic viscosity in Ns/m^2; ρ the gas density in kg/m^3; and H the fracture height assumed to be 1 m for this two dimensional model. Fig. 4 illustrates the applied pressure gradient from boundary B3 to B1 with indication of the flow direction. With this approach, the velocity values and directions are obtained for each fracture in the network.

2.5. Model assumptions

The followings are key assumptions that should be noted for this study:

1. The shale gas well is modeled as methane since it is the predominant constituent.

2. A uniform strata generation rate is assumed for all fractures in the sample DFN model.
3. The fracture length represents the effective length, and the tortuosity effect is ignored.
4. The fractures are modeled assuming transport characteristics through air.
5. A uniform advection velocity with indicated flow direction is used for the sample DFN study.

3. Results and discussions for low-velocity transport

This section discusses the results for the single fracture in Fig. 3 and the sample DFN model in Fig. 4 based on the analytical modeling. The modeling parameters used for the single fracture model (Section 3.1) are itemized in Table 1. The values of c_0 and c_L are hypothetical values used to represent 100% concentration for c_0 and 1% concentration for c_L. Though the value of c_0 seems high, it represents a peak subsurface concentration of methane at the mine depth as studies on methane emissions/content with depth have shown methane values greater than 10 m^3/t coal in a dry ash free state [58–60].

3.1. Result of flux through a single fracture

Fig. 5 shows the impact of fracture length on methane flux for different strata gas emission rates (q) [43,61]. For a non-gassy stratum, $q = 0$, it is observed that the flux decreases with an increase in fracture length until about 100 m, beyond which the flux changes are negligible. It is difficult to make conclusions from this observation, since an important parameter that could vary is the advection velocity (Table 1). Therefore, a study on non-gassy strata is conducted considering different advection velocities as shown in Fig. 6. Two different trends are observed in Fig. 6 based on the velocity range. At very low velocities ($u = 1 \times 10^{-8} - 1 \times 10^{-7}$ m/s) the flux continues to decrease with an increase in fracture length because the flux is dominated by diffusion. However, as the velocity increases, there is a point beyond which the flux is relatively constant as the fracture length increases. For $u = 1 \times 10^{-6}$ m/s, the flux is constant beyond 100 m, and for $u = 1 \times 10^{-5}$ m/s, the flux is constant beyond 10 m. Hence, the flux trend for non-gassy strata is very sensitive to the advection velocity of the leaked gas. This gives an insight into the domain size for sampling or identifying high-risk locations and, in the event of a leak, this information could be used to determine the important locations for sampling to determine associated risk downstream.

For gassy strata, Fig. 5 shows the changes in methane flux with fracture length considering different strata generation rates. For $q = 2.1 \times 10^{-6}$ kg/m^3s, the flux decreases with an increase in fracture length; however, beyond 100 m, the flux shows an increasing trend. At this point, the methane generated from the fracture walls is sufficient to gradually increase the overall flux. Similarly, the same observation is demonstrated for $q = 2.1 \times 10^{-4}$ kg/m^3s and $q = 2.1 \times 10^{-2}$ kg/m^3s. However, the changes in trend occur at different fracture lengths based on the methane generation rate of the stratum. Therefore, the methane generation rate within the surrounding strata is critical at determining the gas flux and associated risk in the case of a failure. Based on this finding, the flux downstream from the leak source

could be higher as methane is generated from the strata. Therefore, the risk associated with well casing failure is more serious if the overlying strata is gassy. Similarly, as described in the Section 1, mining-induced formation changes affect the strata's permeability, which affects the aperture size and the advection velocity. So, the gas flux changes with different advection velocities were investigated for gassy strata as shown in Fig. 7. The values used for this computation are tabulated in Table 2, noting a constant gas generation rate. The trend follows a similar pattern as the gassy strata plot in Fig. 5. However, the influence of advection velocity diminishes as the fracture length increases.

3.2. Result of flux through a discrete fracture network

This section presents the implementation of the method outlined in Section 2.3 for the sample DFN model in Fig. 4. Assuming a gas leak close to boundary B3 (in Fig. 3), a pressure and concentration gradient is induced, and the gas influx is expected from nodes 4–13 and 5–11. For a known boundary concentration as described in Section 2.3, the internal node concentrations and individual fracture flux are obtained from Eqs. (12) and (4), respectively. Table 2 summarizes the fracture length, advection velocities, node concentrations, and the gas flux for Fig. 4. A negative flux/velocity indicates that the flow is in an opposite direction, i.e. $i–j$ instead of $j–i$. After obtaining the results, the model is verified by ensuring that the total flux is zero, and methane mass flow rate is calculated. Assuming a uniform boundary aperture of 1 mm, the mass flow rate through boundary B4 is 7.36×10^{-3} kg/m^{2}s $\times$ 10^{-3} m^2 + 8.35×10^{-3} kg/m^{2}s $\times$ 10^{-3} m^2 = 1.57×10^{-5} kg/s.

This calculated mass flow rate seems relatively low because there are only two boundary fractures (8–6 and 9–7) connected to B4. However, the fractured zone is often denser with a likelihood of more fractures (internal and external nodes), which increases the fracture areas for methane desorption; a recent study on radon gas shows that, a 10% increase in the fracture density increases the radon boundary flux by a factor 15% [39]. Even though this is different gas, it gives an insight on the impact of fracture density on gas flux and opens up more opportunities for future work on this study. Therefore, the accumulative effect of flux from multiple boundary fractures could impact methane concentration in the gob, which affects the mine ventilation requirements to ensure safety.

4. Conclusions and future work

The National Institute for Occupational Safety and Health (NIOSH) conducts research that reduces the risk of mine disasters, such as those that may occur due to shale gas influx from a sheared gas well. This work focuses on transport from a sheared gas well in a low permeable fractured stratum. From the equations derived, gas transport through a single fracture is studied. The results show that:

1. For non-gassy strata, the gas flux decreases with an increase in fracture length; however, this depends on the advection velocity.
2. For a specific advection velocity in a non-gassy stratum, the gas flux is constant beyond a specific fracture length and could be sufficient to determine the associated downstream flux.

3. For gassy strata, the strata methane generation rate affects the flux trend as the fracture length increases. Beyond specific fracture length, the accumulation of the desorbed gas increases the gas flux (or potential mine inflow), which increases the associated risk. However, the extent of the impact is dependent on the advection velocity of the shale gas.

In addition, this work verified the application of this method to a discrete fracture network for determining the boundary flux, which gives an insight into the gas transport. The DFN analysis demonstrates that: the derived equations could be extended to study methane transport through a fracture network; the concentrations of the gas within the strata, which is not accessible for measurements, could be determined using this approach as shown in Table 2; and the combination of this analysis with a site fracture data could be used to determine high concentration zones for installation of gob ventilation boreholes (GVB) to prevent gas inflow to the mine.

In reality, DFN models are often stochastic with fracture lengths, aperture, and fracture orientation generated from statistical distribution; however, only a sample DFN model is analyzed in the current research. The next phase of this study will: (1) refine the assumptions described in Section 2.5 with non-uniform parameters along with pulse methane leakage scenarios where c_0 could vary, (2) consider cases when the fractures are filled with water, (3) introduce stress-based aperture distribution, and (4) expand the application of the derived equations to a stochastically generated DFN model with consideration of uncertainties related to the parameters. However, the findings presented in this study provide an in-depth understanding of the gas transport and the necessary steps to proactively design the ventilation system for the safety of mine workers in the event of a nearby breached well.

References

[1]. Zhang L, Anderson N, Dilmore R, Soeder DJ, Bromhal G. Leakage detection of Marcellus shale natural gas at an upper Devonian gas monitoring well: A 3-D numerical modeling approach. Environ Sci Technol2014;48(18):10795–803. [PubMed: 25144442]

[2]. Soeder DJ, Sharma S, Pekney N, Hopkinson L, Dilmore R, Kutchko B, et al.An approach for assessing engineering risk from shale gas wells in the United States. Int J Coal Geol2014;126:4–19.

[3]. Soeder DJ, Kappel WM. Water resources and natural gas production from the Marcellus Shale. Fact Sheet 2009–3032. Reston, VA: US Geological Survey; 2009.

[4]. Engelder T, Zevenbergen JF. Analysis of a gas explosion in Dimock PA (USA) during fracking operations in the Marcellus gas shale. Process Saf Environ Prot2018;117:61–6.

[5]. Zoback M, Kitasei S, Copithorne B. Addressing the environmental risks from shale gas development. Briefing Paper. Washington, DC: Worldwatch Institute; 2010.

[6]. Rivard C, Lavoie D, Lefebvre R, Séjourné S, Lamontagne C, Duchesne M. An overview of Canadian shale gas production and environmental concerns. Int J Coal Geol2014;126:64–76.

[7]. Ziemkiewicz PF, Quaranta JD, Darnell A, Wise R. Exposure pathways related to shale gas development and procedures for reducing environmental and public risk. J Nat Gas Sci Eng2014;16:77–84.

[8]. Zhang L, Soeder DJ. Modeling of methane migration in shallow aquifers from shale gas well drilling. Groundwater2016;54(3):345–53.

[9]. Warner NR, Christie CA, Jackson RB, Vengosh A. Impacts of shale gas wastewater disposal on water quality in western Pennsylvania. Environ Sci Technol2013;47(20):11849–57. [PubMed: 24087919]

[10]. Vidic RD, Brantley SL, Vandenbossche JM, Yoxtheimer D, Abad JD. Impact of shale gas development on regional water quality. Science2013;340 (6134):1235009. [PubMed: 23687049]

[11]. Ingraffe AR, Wells MT, Santoro RL, Shonkoff SBC. Assessment and risk analysis of casing and cement impairment in oil and gas wells in Pennsylvania, 2000–2012. In: Proceedings of theNational Academy of Sciences of the United States of America. 2014. p. 10955–60.

[12]. Davies RJ, Almond S, Ward RS, Jackson RB, Adams C, Worrall F, et al.Oil and gas wells and their integrity: Implications for shale and unconventional resource exploitation. Mar Pet Geol2014;56:239–54.

[13]. Chafin DT. Sources and migration pathways of natural gas in near-surface ground water beneath the Animas River Valley, Colorado and New Mexico. Water-Resources Investigations Report. 1994. p. 4006.

[14]. Wisen J, Chesnaux R, Wendling G, Werring J, Barbecot F, Baudron P. Assessing the potential of cross-contamination from oil and gas hydraulic fracturing: A case study in northeastern British Columbia, Canada. J Environ Manage2019;246:275–82. [PubMed: 31181476]

[15]. McMahon PB, Thomas JC, Crawford JT, Dornblaser MM, Hunt AG. Methane in groundwater from a leaking gas well, Piceance Basin, Colorado, USA. Sci Total Environ2018;634:791–801. [PubMed: 29653424]

[16]. Li Z, You C, Gonzales M, Wendt AK, Wu F, Brantley SL. Searching for anomalous methane in shallow groundwater near shale gas wells. J Contam Hydrol2016;195:23–30. [PubMed: 27875753]

[17]. Brantley SL, Yoxtheimer D, Arjmand S, Grieve P, Vidic R, Pollak J, et al.Water resource impacts during unconventional shale gas development: The Pennsylvania experience. Int J Coal Geol2014;126:140–56.

[18]. Vengosh A, Warner N, Jackson R, Darrah T. The effects of shale gas exploration and hydraulic fracturing on the quality of water resources in the United States. Procedia Earth Planetary Sci2013;7:863–6.

[19]. Bordeleau G, Rivard C, Lavoie D, Mort A, Ahad J, Malet X, et al.Identifying the source of methane in groundwater in a ‘virgin’ area with regards to shale gas exploitation: A multi-isotope approach. Procedia Earth Planetary Sci2015;13:219–22.

[20]. Allison ML. Hutchinson, Kansas: A geologic detective story. Geotimes2001;46 (10):14–8.

[21]. Su DWH. Effects of longwall-induced stress and deformation on the stability and mechanical integrity of shale gas wells drilled through a longwall abutment pillar. Int J Mining Sci Technol2017;27(1):115–20.

[22]. Coleman JL, Milici RC, Cook TA, Charpentier RR, Kirschbaum M, Klett TR, Pollastro RM, Schenk CJ. Assessment of undiscovered oil and gas resources of the Devonian Marcellus Shale of the Appalachian Basin Province, 2011. Fact Sheet 2011–3092. Reston, VA: US Geological Survey; 2011.

[23]. Ma D, Cai X, Li Q, Duan H. In-situ and numerical investigation of groundwater inrush hazard from grouted karst collapse pillar in longwall mining. Water2018;10(9):1187.

[24]. Guo H, Adhikary DP, Craig MS. Simulation of mine water inflow and gas emission during longwall mining. Rock Mech Rock Eng2009;42(1):25–51.

[25]. Kendorski FS. Effect of high-extraction coal mining on surface and ground waters. In: Proceedings of the12th international conference on ground control in mining. Morgantown, WV; 1993.

[26]. Guo H, Yuan L, Shen B, Qu Q, Xue J. Mining-induced strata stress changes, fractures and gas flow dynamics in multi-seam longwall mining. Int J Rock Mech Min Sci2012;54:129–39.

[27]. Li J, Li F, Hu M, Zhou X, Huo Y. Dynamic monitoring of the mining-induced fractured zone in overburden strata, based on geo-electrical characteristics. Arabian J Geosci2019;12(14):435.

[28]. Cao J, Li W. Numerical simulation of gas migration into mining-induced fracture network in the goaf. Int J Mining Sci Technol2017;27(4):681–5.

[29]. Mucho TP, Diamond WP, Garcia F, Byars JD. Implications of recent NIOSH tracer gas studies on bleeder and gob gas ventilation design. In: Proceedings ofAnnual Meeting of society for Mining, Metallurgy and Exploration. Salt Lake, UT; 2000.

[30]. Adhikary DP, Guo H. Modelling of longwall mining-induced strata permeability change. Rock Mech Rock Eng2015;48(1):345–59.

[31]. Esterhuizen GS, Karacan CO. Development of Numerical Models to InvestigatePermeability Changes and Gas Emission around Longwall Mining Panel. In: Proceedings of the 40th US Symposium on Rock Mechanics (USRMS). American Rock Mechanics Association; 2005.

[32]. Zhang P, Su D. Influence of Longwall Mining on the Stability of Shale Gas Wells in Barrier Pillars. In: Proceedings ofAmerican Rock Mechanics Association. New York; 2019.

[33]. Zhang P, Dougherty H, Su D, Trackemas J, Tulu B. Influence of longwall mining on the stability of gas wells in chain pillars. Int J Mining Sci Technol 2020;30 (1):3–9.

[34]. Chilingar GV, Endres B. Environmental hazards posed by the Los Angeles Basin urban oilfields: an historical perspective of lessons learned. Environ Geol2005;47(2):302–17.

[35]. Safety Mine and Administration Health. CFR § 75.323 Actions for excessive methane. Title 30: Mineral Resources. Electronic Code of Federal Regulations. 2018.

[36]. Bullin KA, Krouskop PE. Compositional variety complicates processing plans for US shale gas. Oil Gas J2009;107(10):50–5.

[37]. Garges JA, Baehr AL. Type curves to determine the relative importance of advection and dispersion for solute and vapor transport. Ground Water1998;36(6):959–65.

[38]. Schatzel SJ, Krog RB, Dougherty H. A field study of US longwall coal mine ventilation and bleeder performance. In: Proceedings ofSME Annual Meeting and Exhibit and CMA 113th National Western Mining Conference 2011. 2011. p. 65–70.

[39]. Ajayi KM, Shahbazi K, Tukkaraja P, Katzenstein K. A discrete model for prediction of radon flux from fractured rocks. J Rock Mech Geotech Eng2018;10(5):879–92.

[40]. Huysmans M, Dassargues A. Review of the use of Péclet numbers to determine the relative importance of advection and diffusion in low permeability environments. Hydrogeol J2005;13(5–6):895–904.

[41]. Bear JModeling flow and contaminant transport in fractured rocks. In Flow and contaminant transport in fractured rocks. 1993. p. 1–37.

[42]. Van Stempvoort D, Maathuis H, Jaworski E, Mayer B, Rich K. Oxidation of fugitive methane in ground water linked to bacterial sulfate reduction. Groundwater2005;43(2):187–99.

[43]. Karacan CÖ. Modeling and prediction of ventilation methane emissions of U.S. longwall mines using supervised artificial neural networks. Int J Coal Geol2008;73(3–4):371–87.

[44]. Lage JL. Contaminant transport through single fracture with porous obstructions. J Fluids Eng, Trans ASME1997;119(1):180–7.

[45]. Tsang YW, Tsang CF. Flow channeling in a single fracture as a two-dimensional strongly heterogeneous permeable medium. Water Resour Res1989;25 (9):2076–80.

[46]. Moreno L, Tsang YW, Tsang CF, Hale FV, Neretnieks I. Flow and tracer transport in a single fracture: A stochastic model and its relation to some field observations. Water Resour Res1988;24(12):2033–48.

[47]. Sudicky EA, Frind EO. Contaminant transport in fractured porous media: Analytical solution for a two-member decay chain in a single fracture. Water Resour Res1984;20(7):1021–9.

[48]. Priest SD. Fluid Flow in Discontinuities. In Discontinuity analysis for rock engineering. Springer Science & Business Media; 2012.

[49]. Renshaw CE. On the relationship between mechanical and hydraulic apertures in rough-walled fractures. J Geophys Res1995;100(B12):24629–5236.

[50]. Cao YB, Feng XT, Yan EC, Chen G, Lü FF, Ji HB, et al.Calculation method and distribution characteristics of fracture hydraulic aperture from field experiments in fractured granite area. Rock Mech Rock Eng2016;49 (5):1629–47.

[51]. Lee HS, Cho TF. Hydraulic characteristics of rough fractures in linear flow under normal and shear load. Rock Mech Rock Eng2002;35(4):299–318.

[52]. Muralidharan V, Chakravarthy D, Putra E, Schechter D. Investigating fracture aperture distributions under various stress conditions using X-ray CT scanner. In: Proceedings of the5th Canadian International Petroleum Conference. Alberta; 2004.

[53]. Zhang C, Jin Z, Song X, Feng G, Li Z, Gao R, et al.Failure mechanism and fracture aperture characteristics of hard thick main roof based on voussoir beam structure in longwall coal mining. Energy Sci Eng 2020;8(2):340–52.

[54]. Bisdom K, Bertotti G, Nick HM. The impact of different aperture distribution models and critical stress criteria on equivalent permeability in fractured rocks. J Geophys Res Solid Earth2016;121(5):4045–63.

[55]. Bisdom K, Bertotti G, Nick HM. A geometrically based method for predicting stress-induced fracture aperture and flow in discrete fracture networks. AAPG Bull2016;100(7):1075–97.

[56]. Klimczak C, Schultz RA, Parashar R, Reeves DM. Cubic law with aperture-length correlation: implications for network scale fluid flow. Hydrogeol J2010;18(4):851–62.

[57]. Zhang X, Sanderson DJ, Harkness RM, Last NC. Evaluation of the 2-D permeability tensor for fractured rock masses. Int J Rock Mech Min Sci1996;33(1):17–37.

[58]. Emission Kędzior S. and commercial utilization of coal mine methane in the Upper Silesian Coal Basin illustrated by the example of Katowice Coal Holding Company. Environ Socio-Econ Stud 2015;3(1):1–10.

[59]. Kędzior S, Dreger M. Methane occurrence, emissions and hazards in the Upper Silesian Coal Basin, Poland. Int J Coal Geol2019;211:103226.

[60]. Tutak M, Brodny J. Forecasting Methane Emissions from Hard Coal Mines Including the Methane Drainage Process. Energies2019;12(20):3840.

[61]. Schatzel SJ, Krog RB, Garcia F, Marshall JK, Trackemas J. Prediction of longwall methane emissions and the associated consequences of increasing longwall face lengths: A case study in the Pittsburgh Coalbed. In: Proceedings of the11th U.S./North American Mine Ventilation Symposium. University Park, PA; 2006. p. 375–82.

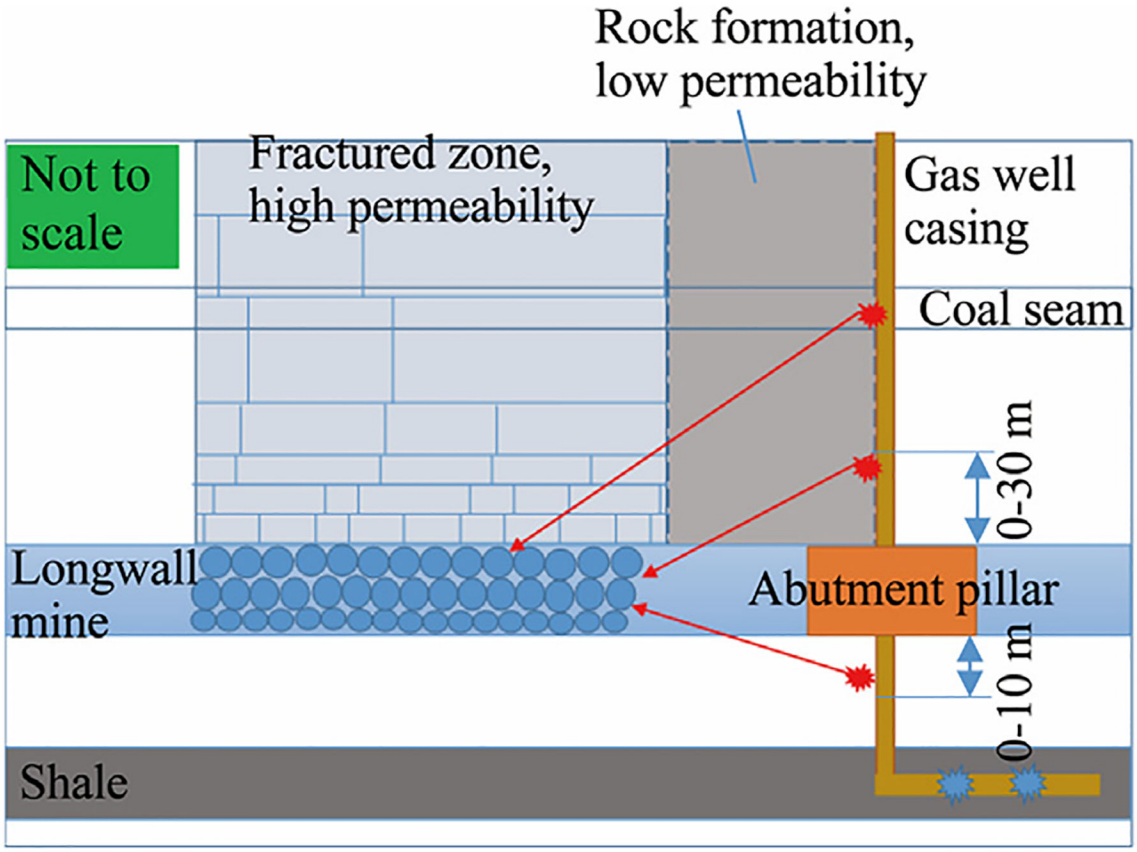

Fig. 1.

Schematic of a site with longwall mine and shale gas well. The arrows indicate potential locations for casing failure and gas transport into the mine. The circles are used to represent caved rocks in the longwall gob.

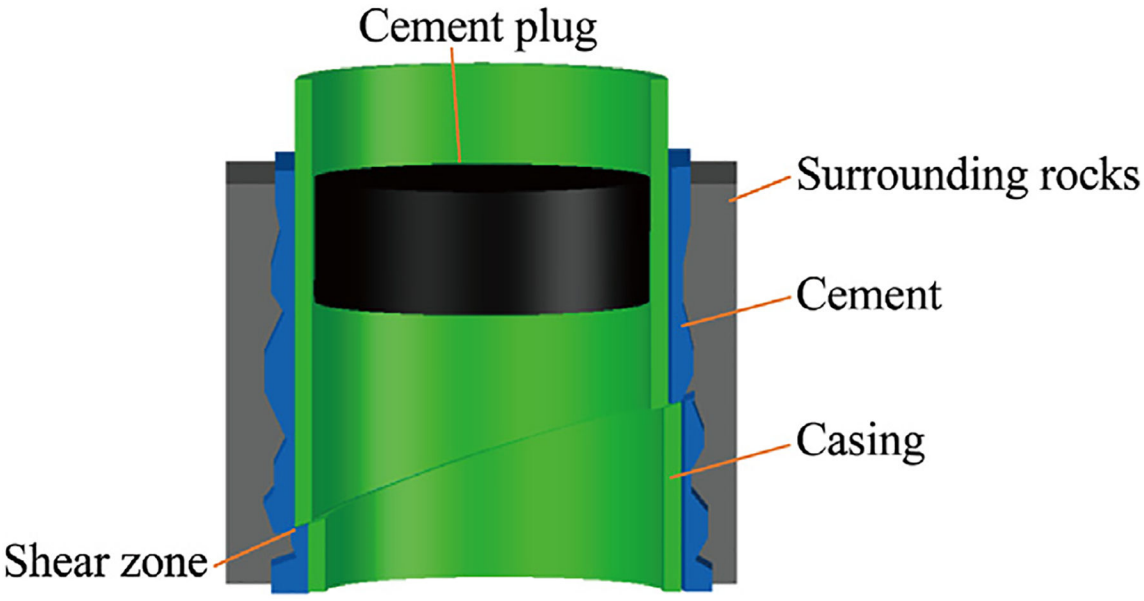

Fig. 2.
Schematic of shear failure for a shale gas well casing.

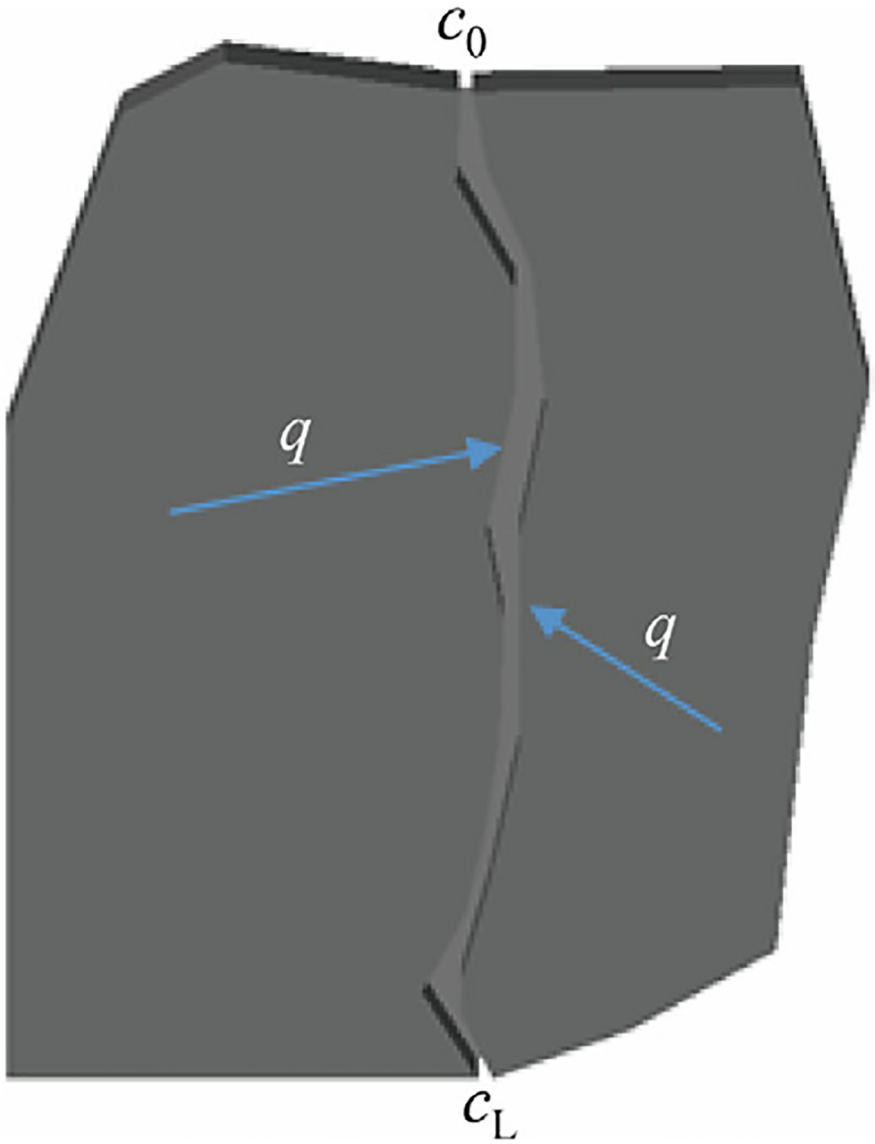

Fig. 3.
Model for transport through a single fracture.

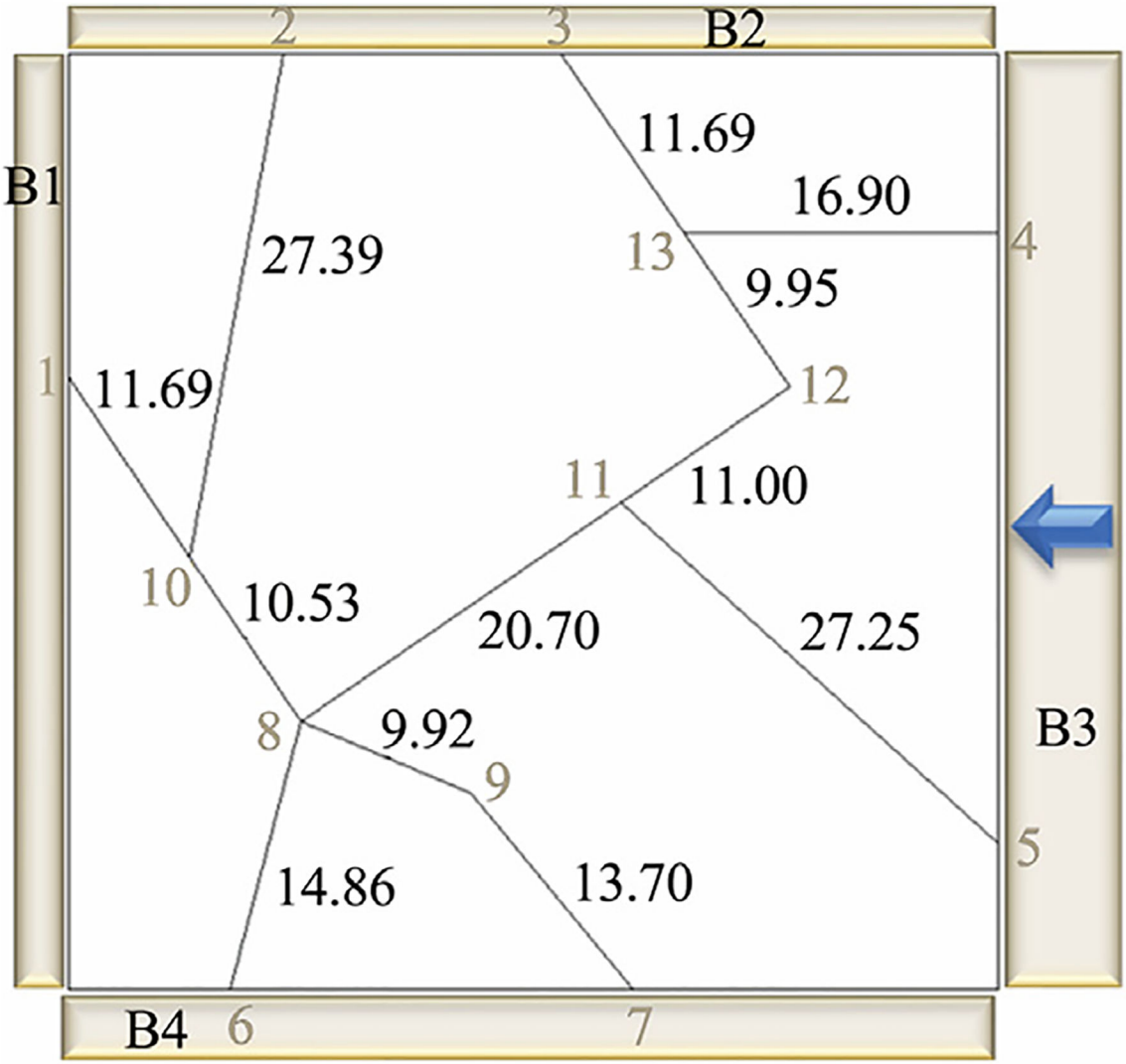

Fig. 4.
Sample DFN model.

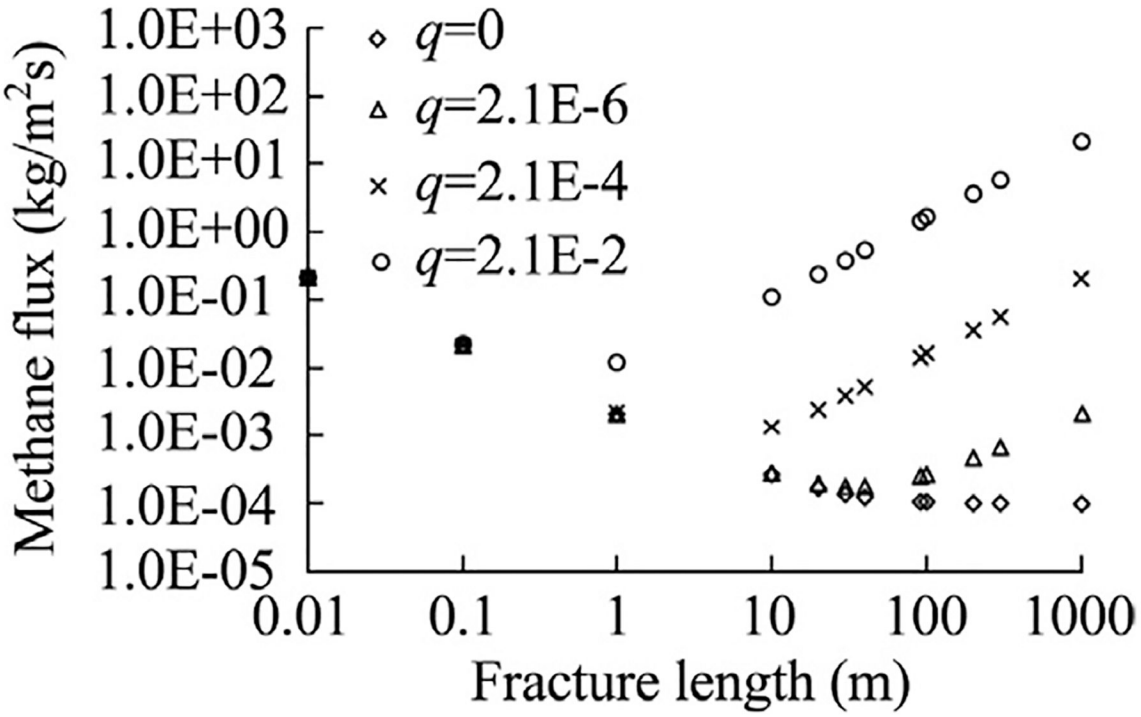

Fig. 5.
Plot of methane flux with fracture length for a non-gassy ($q = 0$) and gassy ($q > 0$) strata.

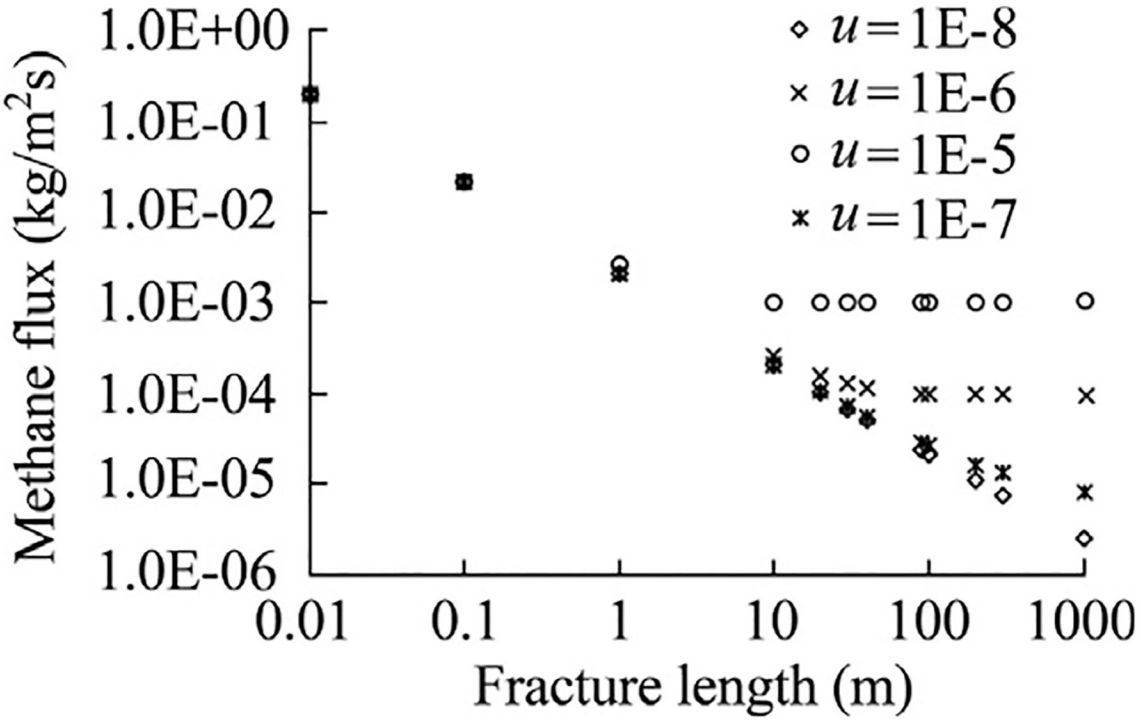

Fig. 6.
Plot of methane flux with fracture length for non-gassy strata at different advection velocities.

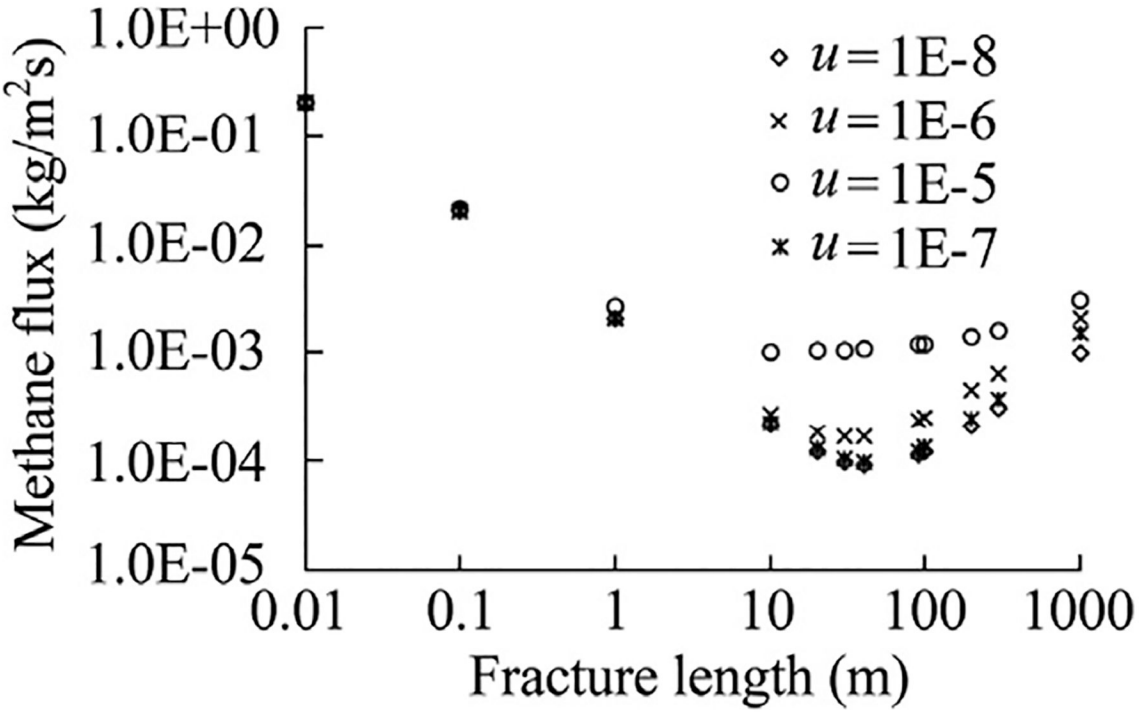

Fig. 7.
Plot of methane flux with fracture length for gassy strata at different advection velocities.

Table 1

Parameters used for analysis in Section 3.1.

Parameter	Value in Fig. 5	Value in Fig. 6	Value in Fig. 7
c_0 (kg/m^3)	100	100	100
c_L (kg/m^3)	1	1	1
D (m^2/s)	2.1×10^{-5}	2.1×10^{-5}	2.1×10^{-5}
u (m/s)	1×10^{-6}	$1 \times 10^{-8} - 1 \times 10^{-5}$	$1 \times 10^{-9} - 1 \times 10^{-5}$
q (kg/m^{3}s)	$0–2.1 \times 10^{-2}$	0	2.1×10^{-6}

Table 2

Parameters for the fracture network in Fig. 4.

Node *j*	Node *i*	Length (m)	Velocity (m/s)	*q* (kg/m^{3}s)	Concentration *j* (kg/m^3)	Concentration *i* (kg/m^3)	Flux (kg/m^{2}s)
10	8	10.53	−1.00E-04	1.00E-04	42.25	73.77	−7.36E-03
6	8	14.86	−1.00E-04	1.00E-04	1.00	73.77	−7.36E-03
9	8	9.92	−1.00E-04	1.00E-04	83.69	73.77	−7.36E-03
11	8	20.79	1.00E-04	1.00E-04	200.09	73.77	2.21E-02
8	9	9.92	1.00E-04	1.00E-04	73.77	83.69	8.35E-03
7	9	13.70	−1.00E-04	1.00E-04	1.00	83.69	−8.35E-03
1	10	11.69	−1.00E-04	1.00E-04	1.00	42.25	−4.20E-03
2	10	27.39	−1.00E-04	1.00E-04	1.00	42.25	−4.20E-03
8	10	10.53	1.00E-04	1.00E-04	73.77	42.25	8.41E-03
8	11	20.79	−1.00E-04	1.00E-04	73.77	200.09	−2.00E-02
12	11	11.00	1.00E-04	1.00E-04	68.51	200.09	7.93E-03
5	11	20.79	1.00E-04	1.00E-04	100.00	200.09	1.21E-02
13	12	9.95	1.00E-04	1.00E-04	58.56	68.51	6.83E-03
11	12	11.00	−1.00E-04	1.00E-04	200.09	68.51	−6.83E-03
12	13	9.95	−1.00E-04	1.00E-04	68.51	58.56	−5.83E-03
3	13	11.69	−1.00E-04	1.00E-04	1.00	58.56	−5.83E-03
4	13	16.90	1.00E-04	1.00E-04	100.00	58.56	1.17E-02
						Sum	0